Line spectroscopy with spatial resolution of laser-plasma X-ray emission

Galimberti M.[1], Giulietti A., Giulietti D.[1], Gizzi L.A., Labate L.[1], Numico R., Salvetti A.

Intense Laser Irradiation Laboratory - IFAM, Area della Ricerca - CNR, Pisa, Italy

Abstract

High dynamic range, space-resolved X-ray spectra of an aluminium laser-plasma in the $5.5 - 8\,\text{Å}$ range were obtained using a TlAP crystal and a cooled CCD camera as a detector. This technique was used to investigate the emission region in the longitudinal direction over a distance of approximately $350\,\mu m$ from the solid target surface. These data show that the electron density profile varies by two order of magnitude with the temperature ranging from about $180\,eV$ in the overdense region to about $650\,eV$ in the underdense region. Accordingly, different equilibria take place across the explored region which can be identified with this experimental technique. Detailed studies on highly ionised atomic species in different plasma conditions can therefore be performed simultaneously under controlled conditions.

1. INTRODUCTION

Plasmas generated by high power, nanosecond laser irradiation of solid targets exhibits a wide range of physical conditions due to the large variation of electron density and temperature both in space and time. In the coronal region, where coupling mechanisms between the laser light and the plasma mostly take place, the atomic physics is dominated by radiative processes and the so-called coronal equilibrium provides a good description of the system independent of the specific structure of energy levels in the plasma. As we go towards the regions of higher electron density, collisions start to contribute and a simple description is no longer possible: a detailed analysis must be performed which takes into account atomic properties, as well as statistical quantities. This so-called collisional-radiative equilibrium can be treated

[1]also at Dipartimento di Fisica, Università di Pisa and INFM, Pisa, Italy

numerically and only for a given set of energy levels. In the densest part of laser plasmas collisions may dominate and local thermodynamic equilibrium may provide again a simple description. On the other hand, once the particular equilibrium is known, X-ray emission can be exploited as a powerful diagnostic tool for characterisation of laser-plasmas (GIULIETTI AND GIZZI 1998) . This is particularly true in the case of very dense plasmas, which cannot be easily studied by other diagnostic techniques like interferometric methods (KAUFFMAN 1991,GRIEM 1997) .

X-ray spectroscopy with spatial resolution allows the plasma parameters like electron temperature, density or ionization state to be measured at different regions. Laser-plasma interaction processes including non-linear interaction phenomena in the underdense region, such as filamentation or self-focusing, two-plasmon decay instability or any other mechanism which affects the electron distribution function significantly, can be studied by X-ray spectroscopy with spatial resolution. Further, spatially resolved spectra can be used to study strongly correlated plasmas of high density (LEBOUCHER-DALIMIER et al. 1993) or the gain region for X-ray lasers (NANTEL 1996). Finally, the knowledge of spatial characteristics of laser produced plasmas allows X-ray sources for applications to be optimised (see (GIULIETTI et al. 1998,MARZI et al. 2000) and references therein).

The main obstacle to an extensive use of this technique is that a micron-scale resolution requires a very narrow slit, with a consequent dramatic reduction of the X-ray flux. For this reason this class of experiments has been limited in the past to relatively low resolution (large slits) and low spectral dispersion. The recent availability of high dynamic range CCD X-ray detectors makes now possible to perform these studies at an unprecedented spatial/spectral resolution, with the possibility of reaching the micron resolution level (X-ray spectro-microscopy). In this report we describe our experimental technique to obtain space resolved spectra of laser-produced plasmas and we show that the combination of a back-illuminated CCD detectors and a flat crystal result in high sensitivity instrument well suited for high spatial/spectral resolution studies of small (10-1000 micrometer) X-ray sources.

2. EXPERIMENTAL SETUP

The experimental setup inside the interaction chamber is shown in Fig. 1. The

plasma was produced by focusing a Nd:YLF laser beam ($\lambda = 1.053\,\mu m$) with an $f/4$ lens onto a rotating cylindrical Al target. The laser, a transversally and longitudinally monomode system, provided an energy up to $3\,J$ in each $3\,ns$ (FWHM) gaussian pulse. Shot to shot fluctuations in the total energy delivered on the target were limited to 10%. The laser beam had a gaussian spatial distribution which resulted in a focal spot size of about $6\,\mu m$ (FWHM) with a Rayleigh length of about $100\,\mu m$, resulting in an intensity on the target up to $5 \times 10^{14}\,W/cm^2$.

A flat *thallium hydrogen phthalate* (TlAP) crystal ($2d = 25.9\,$Å) coupled to a back-illuminated Peltier cooled CCD camera was used to spectrally resolve X-ray emission from the plasma. The crystal, set in a first-order Bragg configuration, and the CCD camera were placed at an angle of 45 degrees with respect to the laser beam axis, i.e. 25 degrees from the plasma expansion axis (see Fig. 1).

The spectrometer allowed the spectral region from 5.5 to 8 Å to be investigated. A typical spatially integrated spectrum in this range, obtained using the set-up of Fig. 1 but without the use of the slit, is shown in Fig. 2. The resonance lines from Al XI (lithium-like), Al XII (helium-like) and Al XIII (hydrogen-like) ions are visible, together with their satellites. Also visible is the intercombination line (IC), which results from the $1s2p\,^3P \rightarrow 1s^2\,^1S$ transition in the Al XII ions. This transition, normally forbidden by the spin selection rule in L-S coupling, becomes allowed due to the mixing of the $1s2p\,^3P$ and $1s2p\,^1P$ states in helium-like ions.

Spectral resolution is determined by the size of the emitting region, by the size of the CCD pixels and by the rocking angle of the crystal. Therefore the resolving power is approximately given by (Hauer et al. 1991)

$$\frac{\lambda}{\delta\lambda} = \sqrt{\frac{\tan^2\vartheta_B}{(\delta\vartheta_c)^2 + (\delta x/L)^2 + (\delta y/L)^2}} \qquad (1)$$

where ϑ_B is the Bragg angle, $\delta\vartheta_c \approx 10^{-4}\,rad$ is the TlAP rocking angle, $L \approx 20\,cm$ is the total distance of the source to the CCD, $\delta x \approx 100\,\mu m$ and $\delta y \approx 24\,\mu m$ are respectively the size of the emitting region and of the CCD pixel. Thus for $\lambda = 7\,$Å we get a resolving power $\lambda/\delta\lambda \approx 5 \times 10^2$, which is dominated by the source size. Notice that the value of $100\,\mu m$ for the source size is just an order of magnitude; actually, the source size depends on the wavelength considered, as shown in the next

section.

The direction perpendicular to the spectral axis in the plane of the CCD matrix can be exploited to spatially resolve the spectrum. In order to accomplish this task a $10\,\mu m$ slit was used (see Fig. 1), which allowed us to obtain spectra with a spatial resolution of about $20\,\mu m$ along the plasma expansion axis.

3. RESULTS AND DISCUSSION

Fig. 3 shows a portion of a typical space resolved spectrum obtained with the set-up of Fig. 1. From this spectrum we can immediately determine the plasma X-ray source longitudinal size, i.e. the size along the main plasma expansion direction, corresponding to the normal to the target surface. Fig. 4 displays the intensity of the Heα line as a function of the distance from the original target surface (hereafter labelled as z). The spatial resolution is about $20\,\mu m$. The size of the emitting region, defined as the FWHM of the Heα intensity profile, is about $280\,\mu m$.

To obtain the plasma electron temperature and density profiles we used the well known method based on the measurement of the ratio between the intensity of two spectral lines. To this purpose, the comparison of measured line ratios with the predictions of the steady state atomic physics code RATION (Lee et al. 1984) was performed. The code was set to calculate atomic populations and line intensities assuming collisional-radiative equilibrium (CRE) for a steady-state, homogeneous plasma of a given size, temperature and density, including opacity effects; a discussion about the applicability of these assumptions to our experimental conditions is given in reference (Macchi et al. 1996). In order to retrieve the electron temperature and density, however, the plasma transverse dimension along the line of sight has to be considered, to take into account the opacity effects. This information can be obtained from spatially integrated spectra, like the one shown in Fig. 2, as we describe in the next subsection.

3.1 Source dimensions and opacity effects

As we have seen above, the source size dominates the spectral resolution $\delta\lambda$, which is much larger than the atomic linewidth, basically due to Doppler and pressure broadening. The size of the emitting region for each spectral line in the direction

of the spectral dispersion can be then determined by the instrumental linewidth. Indeed a spatial extension δx of the source induces a broadening $\delta\lambda_o$ of the observed line at wavelength λ given by

$$\delta\lambda_o = \sqrt{\delta\lambda_c^2 + \left(\frac{\delta x}{L\tan\vartheta_B}\right)^2 \lambda^2} \qquad (2)$$

where ϑ_B and L are as in formula (1) and $\delta\lambda_c = \delta\vartheta_c\,\lambda_B/\tan\vartheta_B$ is the broadening due to the crystal rocking curve. Formula (2) allows the source size δx to be estimated from the line widths $\delta\lambda_o$ knowing $\delta\lambda_c$ and L.

The geometrical parameter L was retrieved with great precision by studying the pattern of the spectral lines in the plane of the CCD matrix. In fact, a given wavelength λ emitted by a point source and dispersed by the crystal is collected in a curved path resulting from the intersection of the CCD matrix plane with a cone having the vertex in the virtual source position. Position and curvature of these paths obviously depend on the geometrical parameters of the spectrometer, including L, which can thus be retrieved by a careful study of the images obtained by the CCD. The finite extent of the source does not affect this consideration, resulting only in a broadening of the lines.

The size of the emitting region was determined for three different spectral lines, namely Heα, Heβ and Lyα. Geometrical considerations, together with the assumption of cylindrical symmetry around the main plasma expansion direction, allowed us to get the transverse, i.e. normal to the expansion axis, size of the emitting regions. The values obtained are $\delta x = 78 \pm 7\,\mu m$, $\delta x = 66 \pm 5\,\mu m$ and $\delta x = 54 \pm 4\,\mu m$ respectively for the Heα, Heβ and Lyα lines. These results show that the size of the emitting region of the hydrogen-like Lyα line is smaller than the corresponding size for the helium-like lines. This is the first evidence of a strong spatial dependence of the electron temperature which affects the distribution of H-like and He-like ions across the plasma.

3.2 Temperature and density profiles

In order to obtain a detailed profile of electron temperature and electron density we measured the spatial behaviour of two line intensity ratios, namely Lyα to Heβ and Heα to IC, from the space resolved spectrum of Fig. 3. The ratio was chosen

because of its strong dependence upon the electron density due to the collisional coupling among the $1s2p$ states of helium-like ions (DUSTON AND DAVIS 1980). Fig. 5 a. and b. show the spatial behaviour of the two line intensity ratios. These data were compared with the predictions of RATION simulations performed assuming different plasma sizes: as an example Fig. 6 displays the Lyα to Heβ intensity ratio as a function of the electron temperature, for different electron densities, obtained assuming a plasma size of $75\,\mu m$.

Comparison with RATION simulations performed for different plasma sizes allowed us to easily estimate the electron density and temperature at the boundaries of the explored region, namely for $z \lesssim 75\,\mu m$ and for $z \gtrsim 200\,\mu m$. This comparison was simplified by the negligible opacity of the plasma in these regions for the selected transitions in our experimental conditions. In particular for $z \gtrsim 200\,\mu m$ we obtained a nearly constant temperature of about $650\,eV$. In contrast, a much lower electron temperature ($\approx 180\,eV$) as well as a density greater than the critical one were estimated for $z \lesssim 75\,\mu m$. Therefore we can expect a strong density and temperature gradients in the intermediate region, although we were not be able to obtain detailed profiles. To overcome this difficulty we used the 1D Lagrangian hydrodynamics code MEDUSA to calculate the density profile in this region (CHRISTIANSEN et al. 1974,RODGERS et al. 1989). The solid curve of Fig. 7 shows the density profile calculated by MEDUSA in our interaction conditions. However, we point out here that the use of a 1D simulation to describe our interaction condition results in a serious overestimation of the electron density for distances from the target plane much greater than the plasma transverse dimension (MAX 1982). Previous studies performed by our group showed in fact a considerable discrepancy between 1D electron density profile simulation and experimental profiles obtained by interferometric techniques (GIZZI et al. 1994). As shown in Fig. 7. in the experimental condition considered in this work MEDUSA simulations performed in a planar geometry give a nearly constant electron density ($\approx 10^{22}\,cm^{-3}$) over the whole $500\,\mu m$ range. This result is in clear disagreement with the results obtained for $z \lesssim 200\,\mu m$, where an electron density of the order of $10^{20}\,cm^{-3}$ can be inferred from the comparison with RATION simulations. We have successfully overcome this problem using an option of MEDUSA to run simulations in a 1D spherical in-

teraction geometry, instead of the planar geometry. In fact, we found that such a geometry resulted in a more reliable prediction of electron density profiles than the planar geometry for distances from the target much greater than the initial plasma transverse dimension size. Here by initial plasma transverse size we refer to the transverse size at the beginning of the plasma formation process, i.e. to the laser focal spot diameter ($\sim 10\,\mu m$). MEDUSA was therefore set to perform hydrodynamic simulations of our experimental conditions by simulating a uniform irradiation of a spherical target. The result is shown in Fig. 7 where the density profiles obtained at the peak of the pulse are shown for three different target radii. The simulation corresponding to a target radius of $100\,\mu m$ provided density values well in agreement with our estimation from spectroscopic measurements in the external regions (for $z \lesssim 75\,\mu m$ and for $z \gtrsim 200\,\mu$). Therefore we used this electron density profile of the plasma to carry out the comparison of the Lyα to Heβ intensity ratio with RATION simulations so as to complete the electron temperature profile in the intermediate region between $z \lesssim 75\,\mu m$ and for $z \gtrsim 200\,\mu m$.

The final temperature profile is shown in Fig. 8. According to the determination from the spatially integrated spectra, a plasma size ranging from 50 to $100\,\mu m$ was used for the region around the critical surface, which is located at about $160\,\mu m$ from the target. For regions closer to the original target position we took into account lower plasma sizes too. However, it is important to point out that in the marginal regions ($z \lesssim 100\,\mu m$ and $z \gtrsim 200\,\mu m$) the uncertainties arising from plasma size determinations result in much lower errors than the experimental ones.

It is interesting to compare the electron temperature profile with an *integrated* temperature determination retrieved from spatially integrated spectra. By performing on these spectra an analysis similar to that described above we were able to estimate an electron temperature of about $260\,eV$. Thus, according to Fig. 8, the electron temperature in the overdense region is slightly lower than the temperature obtained by spatially integrated spectra. In contrast, the temperature rises to much greater values in the coronal region, where the strong laser energy deposition occurs. These results clearly show that space-resolved measurements are indeed necessary in the investigation of laser-produced plasma parameters and in particular in the case of plasma produced by laser interaction with solid targets where strong

temperature/density gradients exist. Additional problems may arise from temporal integration (DUSTON et al. 1983) which still exists in our measurements. However, previous experiments (MACCHI et al. 1996) have demonstrated that X-ray emission intensity closely follows the laser pulse intensity. Therefore we can consider the results of time integrated measurements as characteristic of the peak of the pulse, with time-smearing effects playing only a negligible effect.

4. SUMMARY AND CONCLUSIONS

The use of a space-resolving Bragg X-ray crystal spectrometer equipped with a $10\,\mu m$ slit coupled to a high dynamic range cooled CCD camera allowed us to obtain X-ray spectra with high spatial resolution. This high spatial resolution was only possible thanks to the use of a high sensitivity, high dynamic range cooled CCD detector.

The spectra obtained in these conditions clearly show that large electron temperature and density differences exist in our plasmas over a longitudinal extent of $320\,\mu m$ from the target surface. A temperature profile was obtained which shows that the electron temperature ranges from around $200\,eV$ in the overdense region up to about $650\,eV$ in the coronal region. These results have been compared with the results obtained from spatially integrated spectra which give an *integrated* temperature of approximately $240\,eV$.

Despite the small size of plasmas produced in our experimental conditions, our study clearly demonstrates the effectiveness of our space-resolved measurements in detecting large tempeature and density gradients in a sub-millimetre scale plasma.

References

CHRISTIANSEN J.P., ASHBY D.E., ROBERTS K.V., *Comput. Phys. Commun.* **7**, 271 (1974)

DUSTON D., CLARK R.W., DAVIS J., APRUZESE J.P., *Phys. Rev. A* **27**, 1441 (1983)

DUSTON D., DAVIS J., *Phys. Rev. A* **21**, 1664 (1980)

GIULIETTI A., BENEDUCE C., CECCOTTI T., GIULIETTI D., GIZZI L.A., MILDREN R., *Laser Part. Beams* **16**, 1(1998)

GIULIETTI D., GIZZI L.A., *Riv. Nuovo Cimento* **21**, n.10 (1998)

GIZZI L.A., GIULIETTI D., GIULIETTI A., AFSHAR-RAD T., BIANCALANA V., CHESSA P., DANSON C., SCHIFANO E., VIANA S.M., WILLI O., *Phys. Rev. E* **49**, 5628 (1994)

GRIEM H.R., *Principles of Plasma Spectroscopy* (Cambridge University Press) 1997

HAUER A.A., DELAMATER N.D., KOENIG Z.M., *Laser Part. Beams* **9**, 3 (1991)

KAUFFMAN R., in *Handbook of Plasma Physics*, edited by RUBENCHIK A. and SAGDEEV R.Z. Vol. **3** (North-Holland, Amsterdam) 1991

LEBOUCHER-DALIMIER E., POQUÉRUSSE A., ANGELO P., *Phys. Rev. E* **47**, 1467 (1993)

LEE R.W., WHITTEN B.L., STOUT II R.E., *J. Quant. Spectrosc. Radiat. Transfer* **32**, 91 (1984)

MACCHI A., GIULIETTI D., BASTIANI S., GIULIETTI A., GIZZI L.A., *Nuovo Cimento D* **18**, 727 (1996)

MARZI S., GIULIETTI A., GIULIETTI D., GIZZI L.A., SALVETTI A., *Laser Part. Beams* **18**, 1 (2000)

MAX C.E., in *Laser-Plasma Interaction, Proceedings of the Ecole d'été de physique théorique, Les Houches, session XXXIV*, edited by Balian R. and Adam J.-C. (North-Holland, Amsterdam) 1982

NANTEL M., KLISNICK A., JAMELOT G., HOLDEN P.B., RUS B., CARILLON A., JAEGLÉ P., ZEITOUN PH., TALLENTS G., MACPHEE A.G., LEWIS C.L.S., JACQUEMOT S., BONNET L., *Phys. Rev. E* **54**, 2852 (1996)

RODGERS P.A., ROGOYSKI A.M., ROSE S.J., *RAL Report* No. RAL-89-127, 1989 (unpublished)

Captions

Fig. 1 Schematic set-up of the experiment showing the arrangement of the crystal spectrometer and the geometry of the interaction.

Fig. 2 Spatially integrated spectrum of X-ray radiation in the range from 5.5 to 8 Å emitted by an Al plasma generated from laser irradiation of a solid target.

Fig. 3 Spatially resolved spectrum. x refers to the direction indicated in Fig. 1.

Fig. 4 Measured intensity of the Heα line from the plasma as a function of the distance from the target plane (corresponding to "0"). This plot was obtained from the space resolving spectrograph shown in Fig. 1.

Fig. 5 Measured a) Lyα to Heβ and b) Heα to IC intensity ratios as a function of the distance from the original target position along the plasma main expansion direction.

Fig. 6 Calculated Lyα to Heβ intensity ratio as a function of the electron temperature for a plasma size of 75 μm and for five different electron densities.

Fig. 7 Plasma electron density profiles at the peak of the laser pulse as simulated by MEDUSA in the standard planar geometry (continuous curve) and in the spherical geometry for three values of the target radius (dashed curves).

Fig. 8 Electron temperature profile of the plasma produced by the laser irradiation of a solid Al target by a ns Nd laser. The spatially resolved measurement was carried out using a space-resolving X-ray crystal spectrometer equipped with a high-dynamic range cooled CCD detector.

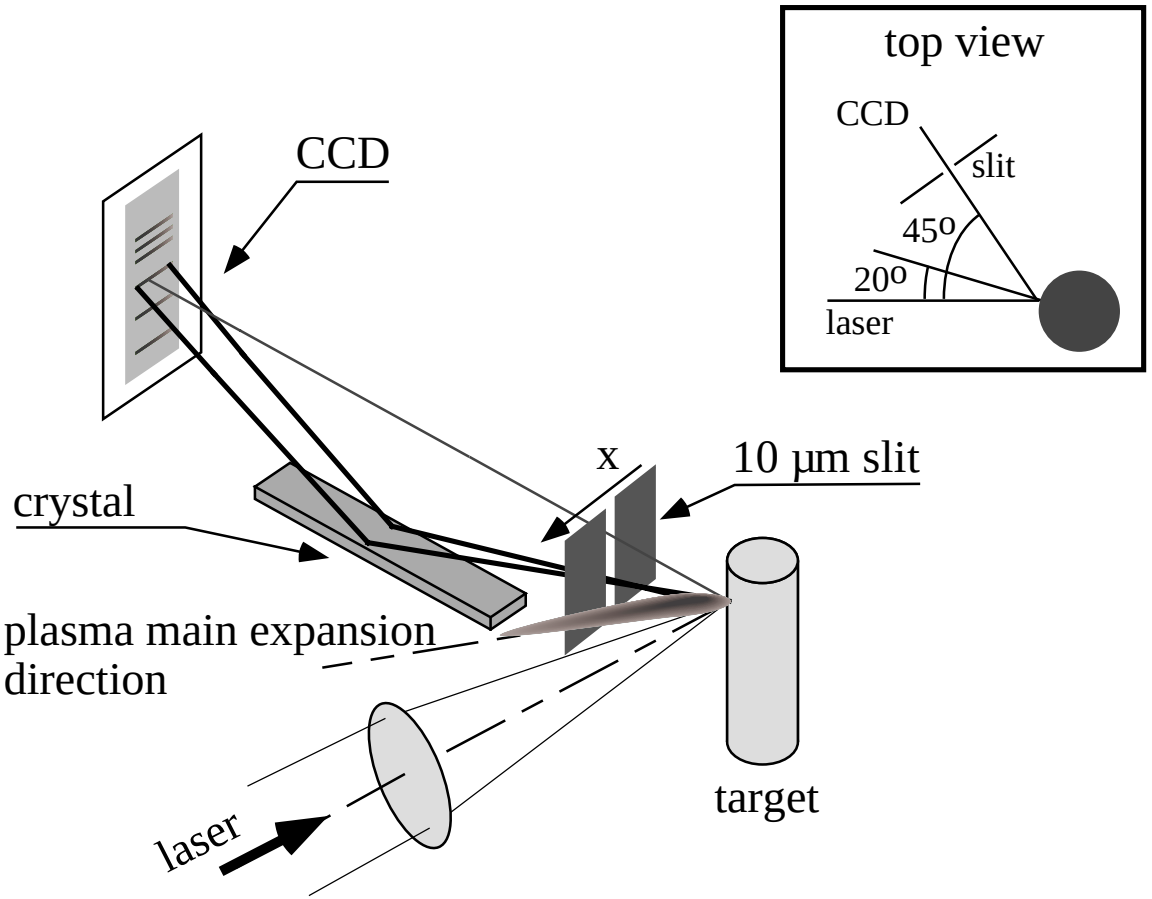
top view
CCD
slit
45º
20º
laser
CCD
x
10 µm slit
crystal
plasma main expansion
direction
laser
target

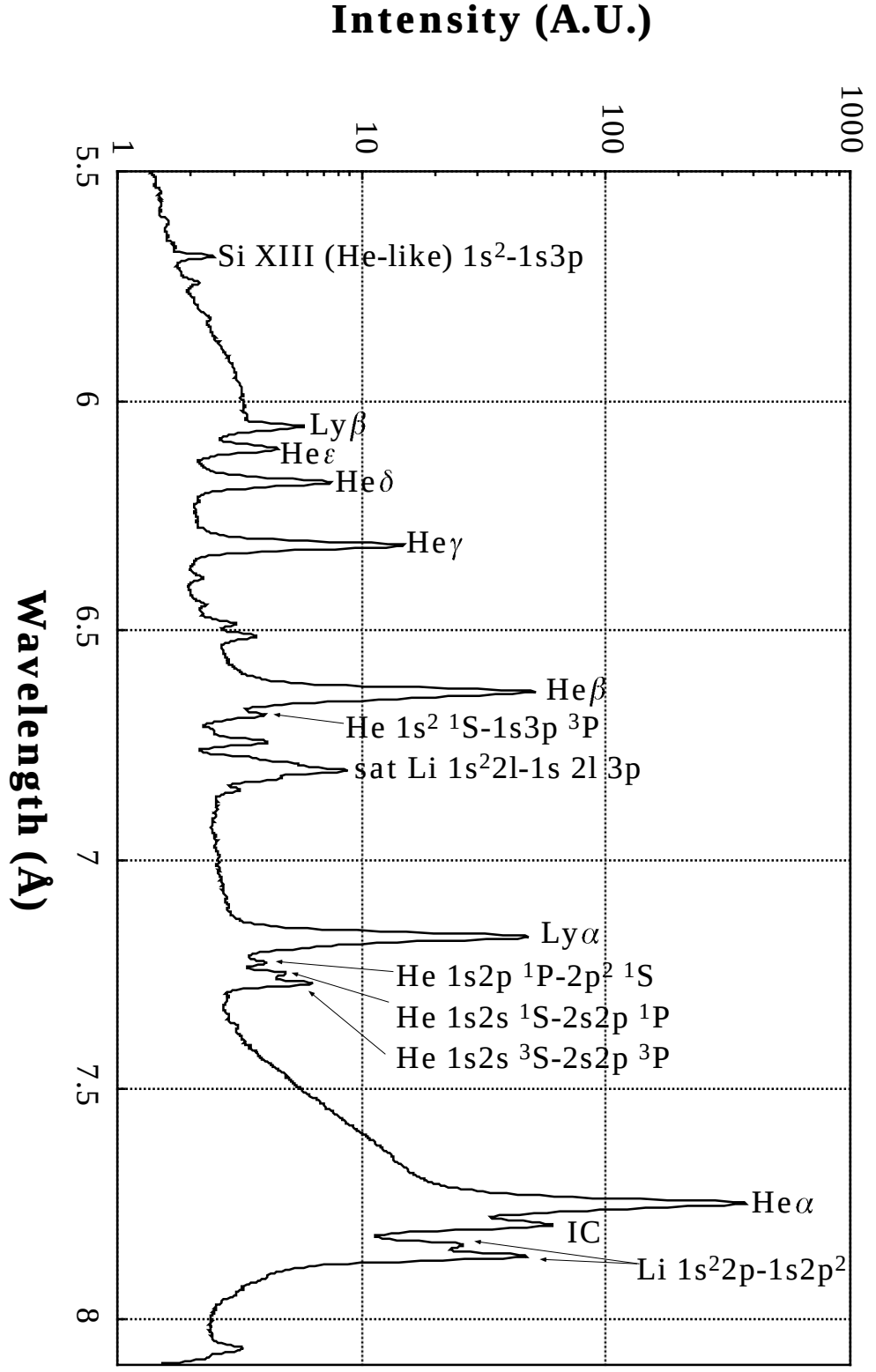
Intensity (A.U.)
1
10
100
1000
Wavelength (Å)
5.5
6
6.5
7
7.5
8
Si XIII (He-like) 1s2-1s3p
Lyβ
Heε
Heδ
Heγ
Heβ
He 1s2 1S-1s3p 3P
sat Li 1s22l-1s 2l 3p
Lyα
He 1s2p 1P-2p2 1S
He 1s2s 1S-2s2p 1P
He 1s2s 3S-2s2p 3P
Heα
IC
Li 1s22p-1s2p2

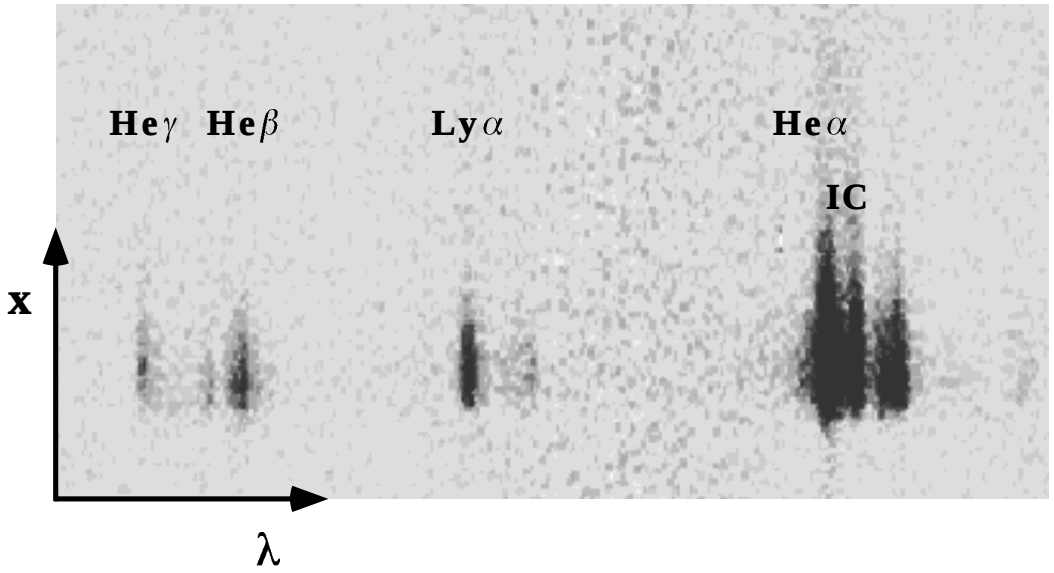
Heγ
Heβ
Lyα
Heα
IC
x
λ

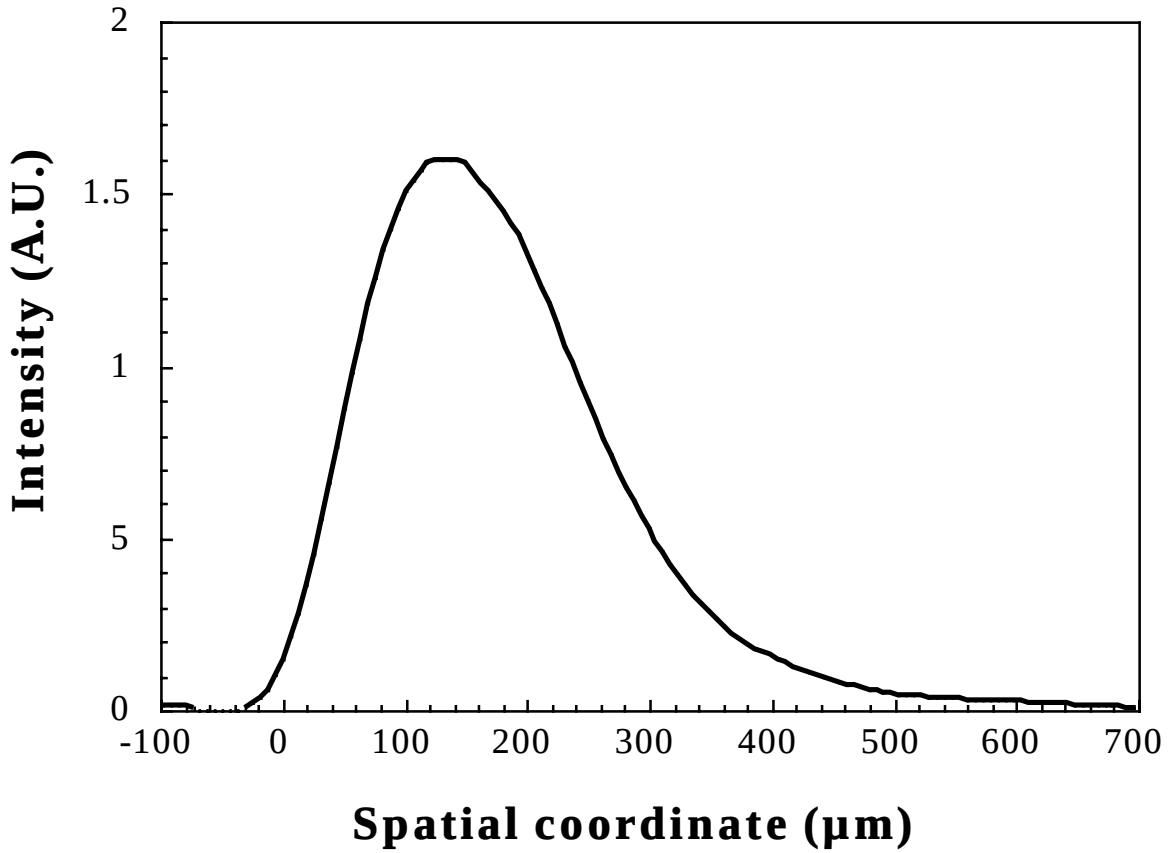
Intensity (A.U.)
2
1.5
1
5
0
-100
0
100
200
300
400
500
600
700
Spatial coordinate (µm)

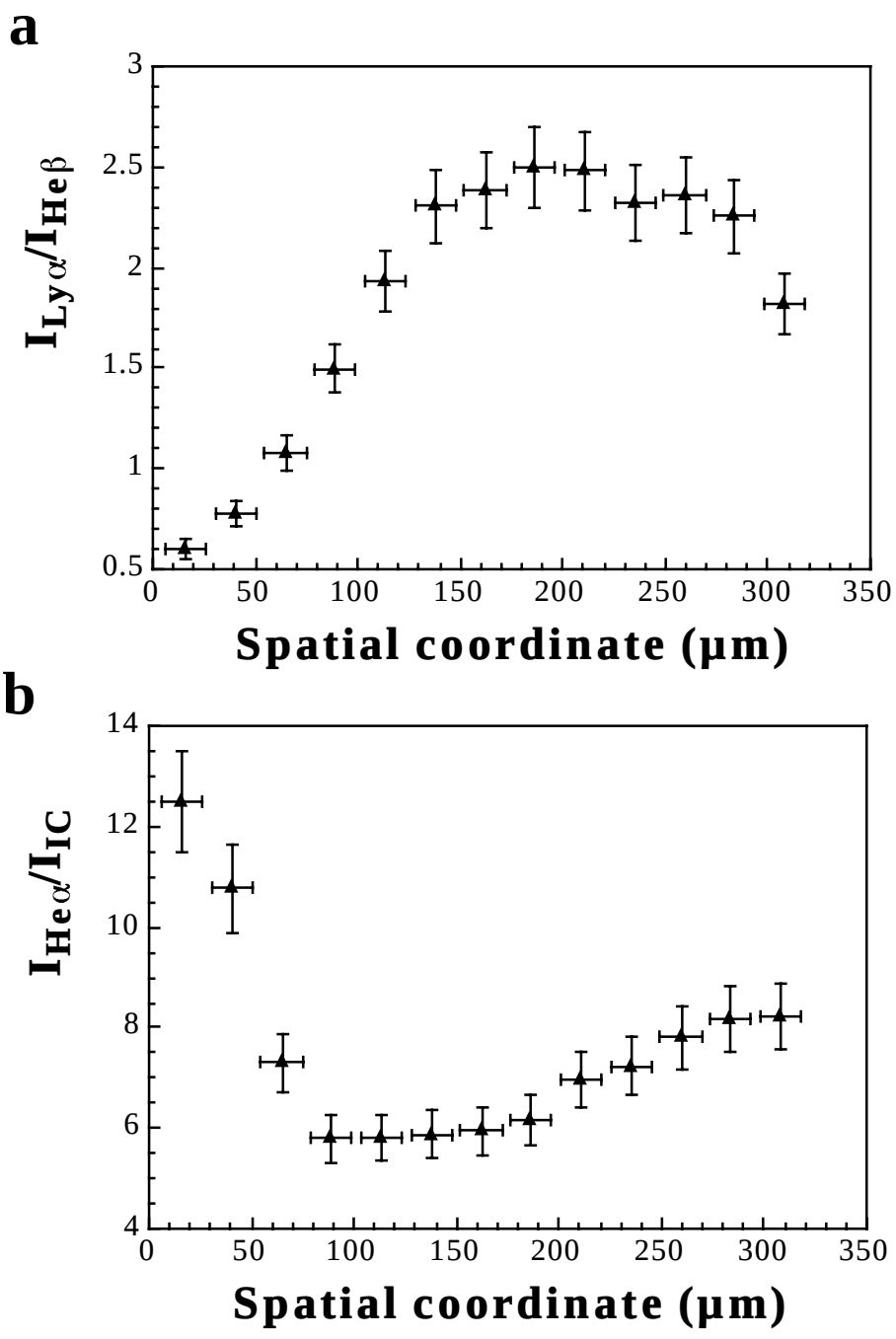
a
$I_{Ly\alpha}/I_{He\beta}$
3
2.5
2
1.5
1
0.5
0
50
100
150
200
250
300
350
Spatial coordinate (μm)
b
$I_{He\alpha}/I_{IC}$
14
12
10
8
6
4
0
50
100
150
200
250
300
350
Spatial coordinate (μm)

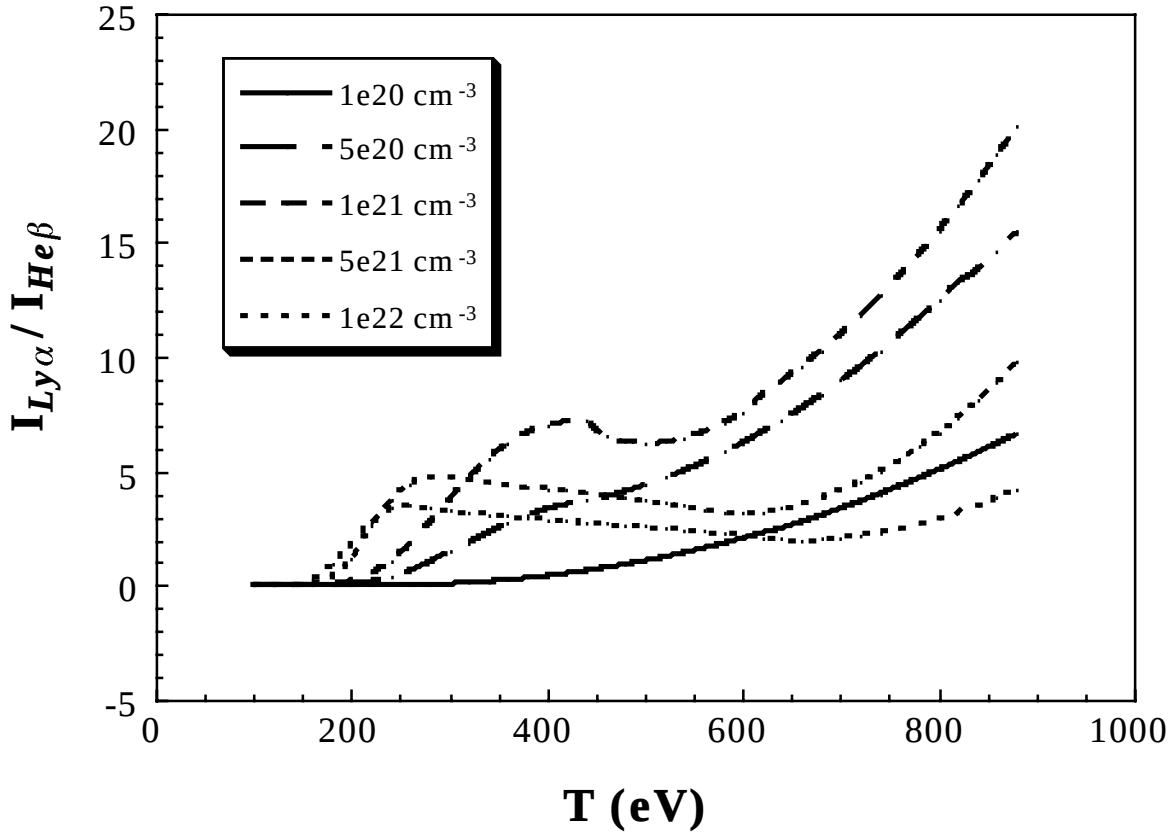
25
20
15
10
5
0
-5
0
200
400
600
800
1000
$I_{Ly\alpha} / I_{He\beta}$
T (eV)
1e20 cm -3
5e20 cm -3
1e21 cm -3
5e21 cm -3
1e22 cm -3

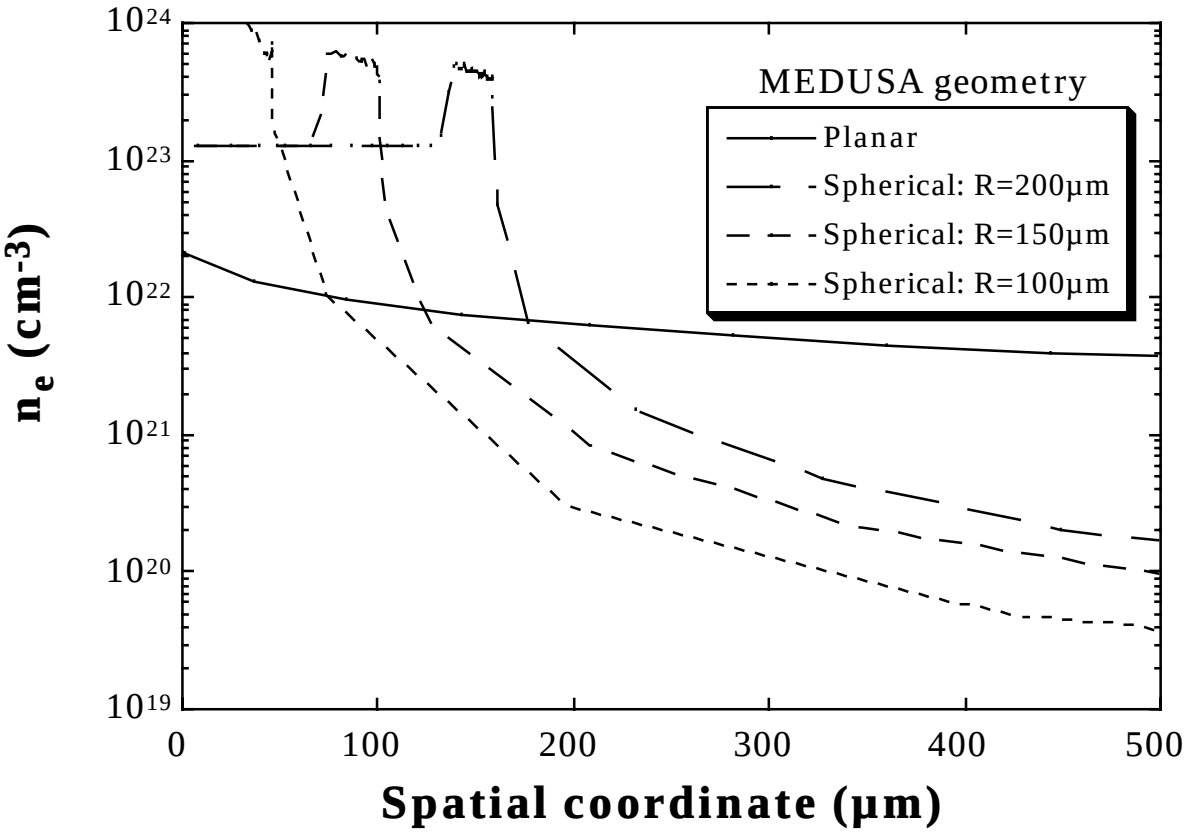
MEDUSA geometry
Planar
Spherical: R=200µm
Spherical: R=150µm
Spherical: R=100µm
10^{24}
10^{23}
10^{22}
10^{21}
10^{20}
10^{19}
n_e (cm^{-3})
0
100
200
300
400
500
Spatial coordinate (µm)

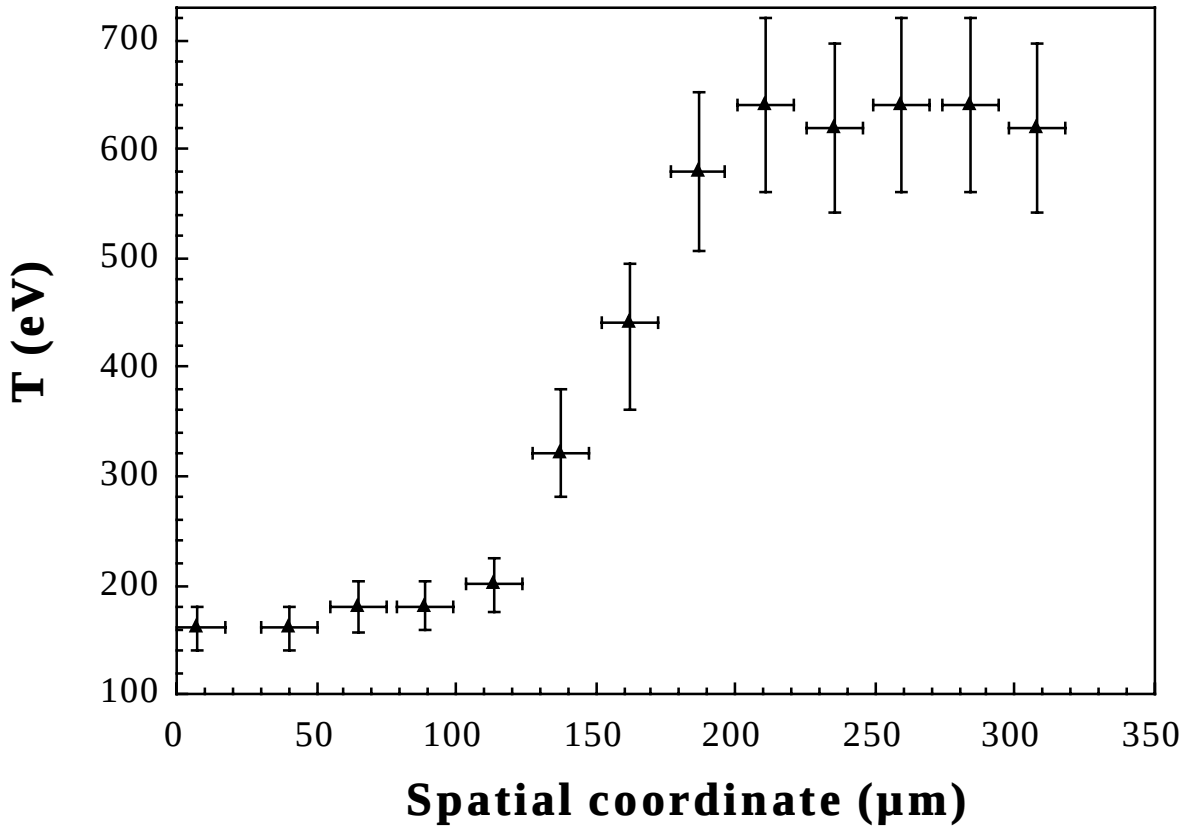
T (eV)
700
600
500
400
300
200
100
0
50
100
150
200
250
300
350
Spatial coordinate (μm)